AGU PUBLICATIONS

Geophysical Research Letters

RESEARCH LETTER
10.1002/2016GL068996

Key Points:
- Semienclosed estuarine seas may be protected from hypoxia but not from ocean acidification
- Significant O_2 uptake occurs during intense tidal mixing in narrows, while little CO_2 is out gassed
- The Strait of Georgia is enriched in carbon and has low pH relative to the surrounding ocean

Supporting Information:
- Supporting Information S1

Correspondence to:
D. Ianson,
debby.ianson@dfo-mpo.gc.ca

Citation:
Ianson, D., S. E. Allen, B. L. Moore-Maley, S. C. Johannessen, and R. W. Macdonald (2016), Vulnerability of a semienclosed estuarine sea to ocean acidification in contrast with hypoxia, *Geophys. Res. Lett.*, *43*, 5793–5801, doi:10.1002/2016GL068996.

Received 6 APR 2016
Accepted 20 MAY 2016
Accepted article online 28 MAY 2016
Published online 11 JUN 2016

Vulnerability of a semienclosed estuarine sea to ocean acidification in contrast with hypoxia

Debby Ianson[1,2], Susan E. Allen[2], Benjamin L. Moore-Maley[2], Sophia C. Johannessen[1], and and Robie W. Macdonald[1]

[1] Institute of Ocean Sciences, Fisheries and Oceans Canada, Sidney, British Columbia, Canada, [2] Department of Earth, Ocean and Atmospheric Science, University of British Columbia, Vancouver, British Columbia, Canada

Abstract The Strait of Georgia (SoG) is a large semienclosed estuary that spatially dominates the Salish Sea on the North American Pacific coast. The region is well populated, harbors significant aquaculture, and is vulnerable to climate change. We present the first inorganic carbon data collected in the SoG covering all seasons (2003 and 2010–2012) and put them into the context of local circulation and oxygen cycles. Results show that the SoG has a higher carbon content and lower pH than surrounding waters. Aragonite saturation horizons in the SoG do not become deeper than 20–30 m and shoal to the surface for extended periods. Furthermore, incoming upwelled "acidified" water from the outer coast actually increases local pH. Finally, intense mixing in the physically restricted channels connecting the SoG to the outer coast allows significant oxygen uptake but minimal CO_2 out gassing, protecting the SoG from hypoxia but not from ocean acidification.

1. Introduction

Anthropogenic ocean acidification (OA) [*Intergovernmental Panel on Climate Change*, 2011], decreasing oxygen (O_2) levels and increasing water temperature (T), pose threats to marine ecosystems that will intensify in the coming decades [*Gruber*, 2011]. Estuaries naturally have unique, highly variable biogeochemical properties with respect to surrounding ocean waters [e.g., *Feely et al.*, 2010; *Waldbusser and Salisbury*, 2014; *Azetsu-Scott et al.*, 2014]. In addition, estuaries often host significant aquaculture, industry, and human populations, all of which may intensify OA and hypoxia [*Cai et al.*, 2011] making these areas particularly vulnerable [*Ekstrom et al.*, 2015].

The Strait of Georgia (SoG) is a large (6800 km^2, > 400 m deep), well-populated, semienclosed estuary that forms the northern reach of the Salish Sea, on the Pacific coast of North America (Figure 1a). Most shellfish harvested in British Columbia (BC), Canada, come from this waterway, and there is significant finfish aquaculture at its northern boundary [*Haigh et al.*, 2015]. Estimates suggest that finfish aquaculture contributes ~10% of the anthropogenic particulate organic carbon (POC) entering the SoG; the majority comes from pulp mills and sewage. These fluxes, however, are dwarfed by the POC load of the Fraser River (FR) [*Johannessen et al.*, 2014].

Carbon and oxygen cycles are tightly linked through photosynthesis, respiration, and remineralization but decoupled in air-sea gas exchange. Although CO_2 is a reactive gas, its hydration/dehydration kinetics are slow so its air-sea transfer rate is not chemically enhanced [*Emerson and Hedges*, 2008] and it reaches equilibrium much more slowly than does O_2 [e.g., *Zhai et al.*, 2009]. We focus on the decoupling of these cycles, especially gas exchange in the dynamic Haro region (Figure 1a) and how it may change in the next decades.

Here we present the first data from which the carbonate system may be fully defined in the SoG, including connecting waters (Figure 1). These data cover all seasons and include strong and weak Fraser freshet years (Table S1 in the supporting information). Saturation states with respect to the shellfish-relevant, aragonitic form of calcium carbonate (Ω_a), [*Waldbusser et al.*, 2015], and the depth (below surface) of the aragonite saturation horizon ($\Omega_a = 1.0$) above which conditions are considered biologically "favorable" [*Feely et al.*, 2008] are estimated. We contrast seasonal pH and Ω_a cycles in surface waters by region and by strength of freshet and characterize the summer inorganic carbon content of key water masses in the region.

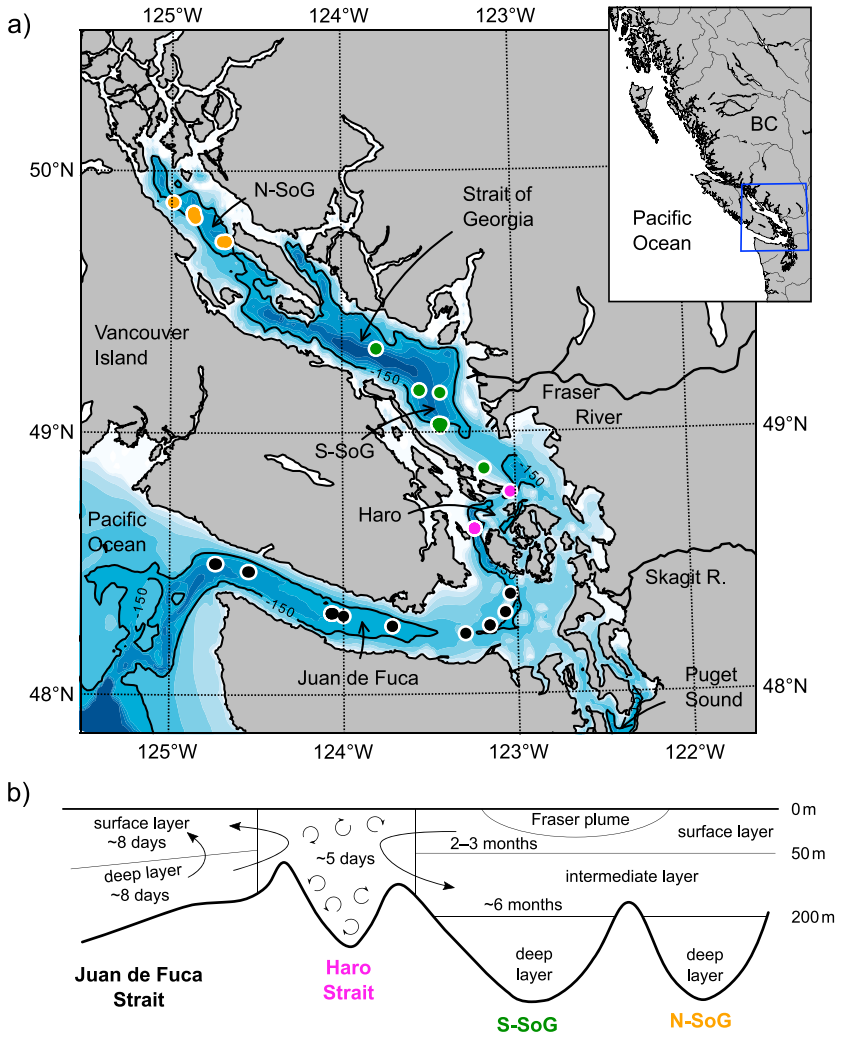

Figure 1. (a) Map with sampling locations colored by region: north-SoG (orange), south-SoG (green), Haro (purple), and Juan de Fuca (black). Blue indicates bathymetry; deeper is darker. The 150 m isobath roughly indicates the location of major sills. (b) Circulation cartoon, adapted from R. Pawlowicz, personal communication, 2014.

1.1. Oceanography of the Strait of Georgia

Tides and estuarine circulation, driven primarily by the glaciofluvial FR, control the main circulation in the SoG [*LeBlond*, 1983]. The SoG is bounded at the north and south by narrow channels with sills between islands (Figure 1a). Primary exchange with the open ocean occurs at the southern end via the Haro region [*Pawlowicz et al.*, 2007], which includes Haro Strait. The large tidal range (~4 m) drives intense mixing in Haro [*Farmer et al.*, 2002]. As a result Haro couples the strong estuarine circulation cells of Juan de Fuca Strait (JdF) and the SoG (Figure 1b). Most of the outer Pacific water drawn into the subsurface JdF as estuarine return flow goes back out to sea in the JdF surface layer. The return estuarine flow entering the SoG is a heavily modified mix of the remaining subsurface Pacific water and surface SoG water [*Pawlowicz et al.*, 2007]. This return flow enters the SoG at about 100 m [*Masson*, 2006, hereafter M06] throughout the year.

There are two deep (>300 m) basins in the SoG: the northern basin (N-SoG) and the larger southern basin (S-SoG), which includes the mouth of the FR (Figure 1). Both basins are heavily stratified, with the brackish Fraser plume (top 2–10 m) in the S-SoG sliding overtop the 50 m thick upper layer. This layer has a residence time (τ) of a few months. Below that, the intermediate layer ($\tau \sim 6$ months), which receives continual estuarine return flow extends to a depth of 200 m [*Pawlowicz et al.*, 2007]. The deep SoG layer is relatively stagnant ($\tau >1$ year), receiving deep water renewal in discrete pulses, mainly during spring and fall [*Masson*, 2002; *Pawlowicz et al.*, 2007].

The FR also influences local chemistry. It contains products from both carbonate and silicate weathering [*Voss et al.*, 2014]. Thus, total alkalinity (TA) in the FR is significant (500–1350 μmol kg^{-1}) and is dominated by carbonate alkalinity [*Moore-Maley*, 2014], which may help buffer CO_2, reducing OA [*Hu and Cai*, 2013]. Silicic acid, $Si(OH)_4$, is plentiful throughout the SoG, contributing to high productivity and a strong spring diatom bloom [*Harrison et al.*, 1983].

2. Methods

Dissolved inorganic carbon (DIC) and TA data were collected on 16 cruises (Table S1) along with T, salinity (S), discrete O_2, and nutrient data and used to define the carbonate system (Text S1) after careful quality control (Text S2).

2.1. Seasons

We partition these data into five seasons: winter (November–February), spring (March to mid-May), freshet (defined below), summer (mid-May to September), and fall (October–November), consistent with the large-scale wind patterns responsible for upwelling/downwelling (Table S2) [*Bylhouwer et al.*, 2013]. The transition to downwelling coincides with the first winter storms, which mix down the strong summer surface stratification in the SoG. Upwelling and downwelling on the outer coast directly influence the properties of the subsurface inflow in the JdF [M06; *Davis et al.*, 2014]. The freshet "season" occurs within the summer season, in years when the Fraser outflow is strong enough to produce surface $S < 20$ at our sampling locations in the S-SoG (Figure 1; 2011 and 2012 in our data).

2.2. Gas Flux and Inventories in the Haro Region

In Haro, net air-sea CO_2 and O_2 exchange was estimated by integrating hourly fluxes over the local residence time (Text S3) each time Haro was sampled (Table S3). Total water column DIC and O_2 inventories and *disequilibrium* inventories (DIC surplus, O_2 deficit, relative to the atmosphere) within Haro were also estimated (Text S3). The fraction of this disequilibrium inventory that is erased by gas flux during passage through Haro was then computed (Table S4).

2.3. Determining Summer DIC Water Mass End-Members

DIC end-members associated with each water mass influencing the region in summer [M06], subsurface Pacific or deep JdF (*d*JdF), FR-plume, deep S-SoG (*d*S-SoG), and deep N-SoG (*d*N-SoG), were estimated using the strong regional DIC-S relationships. Positions in DIC-S space relative to mixing lines defined by these end-members were compared (Text S4 and Tables S5 and S6).

3. Results and Discussion

3.1. Water Properties

Water properties (DIC, pH, and O_2) in the SoG are distinct from those outside (Figures 2a–2c). Meanwhile, properties in Haro lie between those in the SoG and JdF. Since S controls density in this region, we discuss these differences with reference to S; potential density (σ_θ) plots look nearly identical (Figure S1). In contrast, TA-S properties do not vary with region (Figure 2d).

Dilution and mixing exert strong control over DIC in each region (DIC is roughly linear with S—Figure 2a). However, there is more DIC in the SoG at the same S (or density) than outside in Haro and JdF (excepting a single deep water intrusion event below 300 m in the S-SoG (Figure S2); green asterisk—Figure 2). Similarly, pH is significantly lower in the SoG at the same S (Figure 2b). At the S associated with estuarine return flow into the S-SoG ($S = 30.3$; $\sigma_\theta \sim 23.5$), pH is lower (~0.3) in the SoG than in JdF. Furthermore, the lowest pH levels inside the SoG (~7.5) are lower (by ~0.05 pH units) than anywhere in JdF or Haro (Figure 2b). Biological fluxes exert significant control over pH. Also, unlike DIC, pH is not conservative with changes in S (or T).

Air-sea exchange of O_2 is rapid, and biological fluxes are large relative to the O_2 inventory, so O_2 is not as strongly governed by mixing/dilution as is DIC. Like pH, O_2 in the SoG is significantly lower (~100 μmol kg^{-1}) at S associated with water entering the SoG ($S = 30.3$) than outside. However, in contrast to pH, the lowest O_2 in the region is found in JdF (60 μmol kg^{-1}; Figure 2c). In the deep SoG, O_2 is always >100 μmol kg^{-1}, still well above hypoxic thresholds (~70 μmol kg^{-1}, estimated from a 5 kPa partial pressure of oxygen [*Seibel*, 2011] and local T, S) for marine organisms that spend time in low O_2 conditions. The intense mixing in Haro is responsible for this feature.

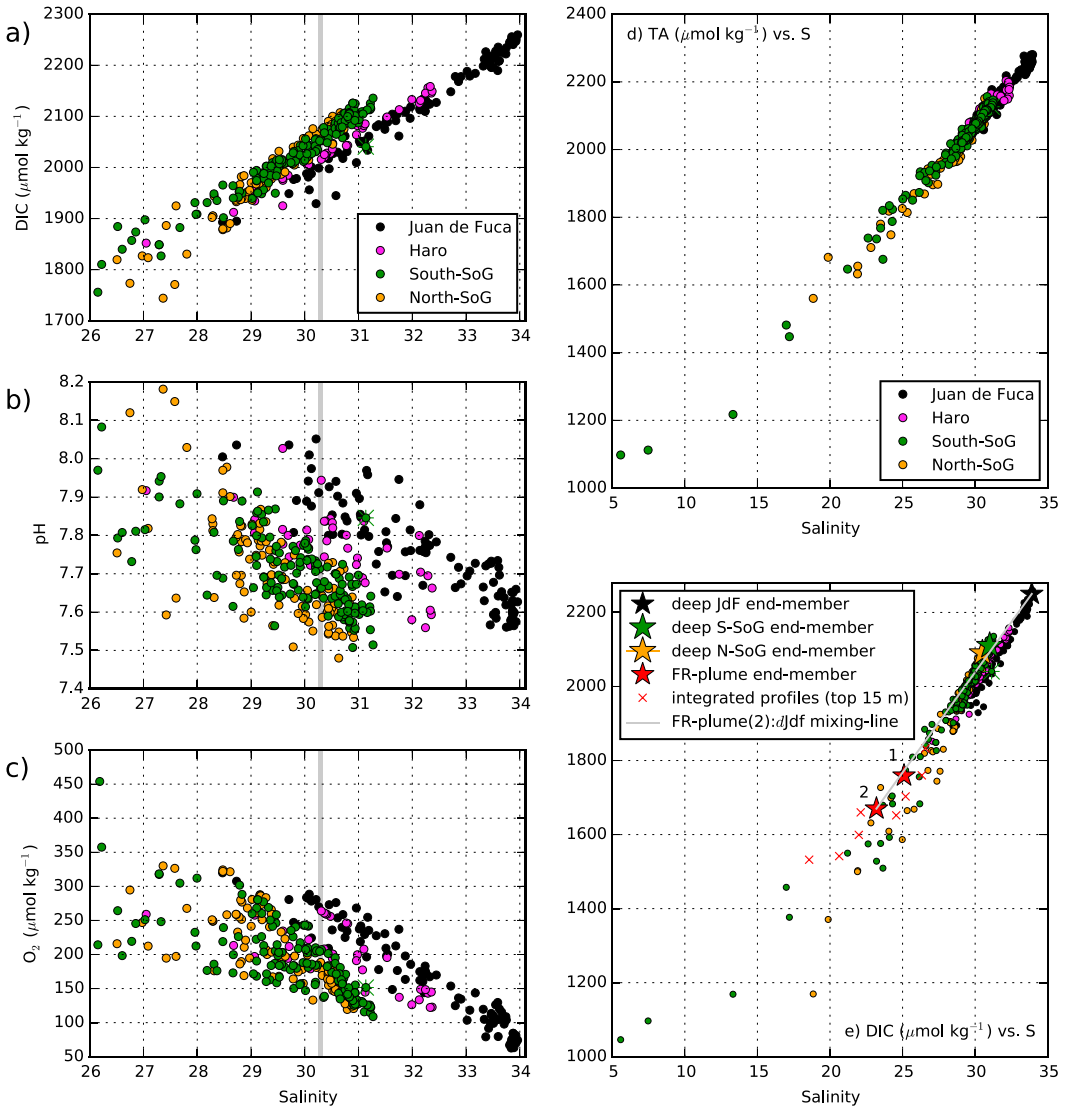

Figure 2. (a, e) DIC, (b) pH, (c) O_2, and (d) TA versus S (PSS-78) colored by region. Uncertainty in DIC, O_2, and TA is smaller than symbol diameter. Uncertainty in pH (estimated from DIC and TA) is <0.036, S>31; <0.038, 26<S<31. The grey vertical line indicates S = 30.3 ($\sigma_\theta \sim 23.5$) associated with water entering the SoG from Haro (~100 m). The green asterisk marks a deep water intrusion from Haro to the S-SoG (Figure S2). (e) Stars mark summer DIC end-members; FR-plume end-member was estimated in two ways—(1) as the others (Table S5) and (2) mean of integrated individual profiles (red x) (Table S6).

3.2. Ventilation in Haro Strait

Tidal mixing is so strong in Haro Strait that the full water column (> 200 m) is poorly stratified (Figures 3a and 3b) regardless of time within the spring-neap tidal cycle (Table S3). Stratification is at a minimum in spring season because downwelling has filled the outer shelf with less dense, offshore surface water that feeds the subsurface JdF return flow, and surface water entering Haro from the SoG is relatively dense (prefreshet) [*Masson*, 2002]. As a result, the water column is well ventilated. Bottom O_2 in Haro is high and near equilibrium with the atmosphere (>240 μmol kg^{-1} and within 20% of saturation, April—Figure 3a), and water column inventories (Text S3) are at a maximum (Table S4). Once the upwelling season and the freshet begin, more energy is required to mix the water column, so Haro becomes weakly stratified. Also, the subsurface JdF return flow (upwelled water) has low O_2 (40% less than in winter) [*Masson*, 2006] and so O_2 inventories are reduced (~35%, Table S4 and Figure 3a). However, bottom O_2 is still relatively high (>120 μmol kg^{-1}, September—Figure 3a).

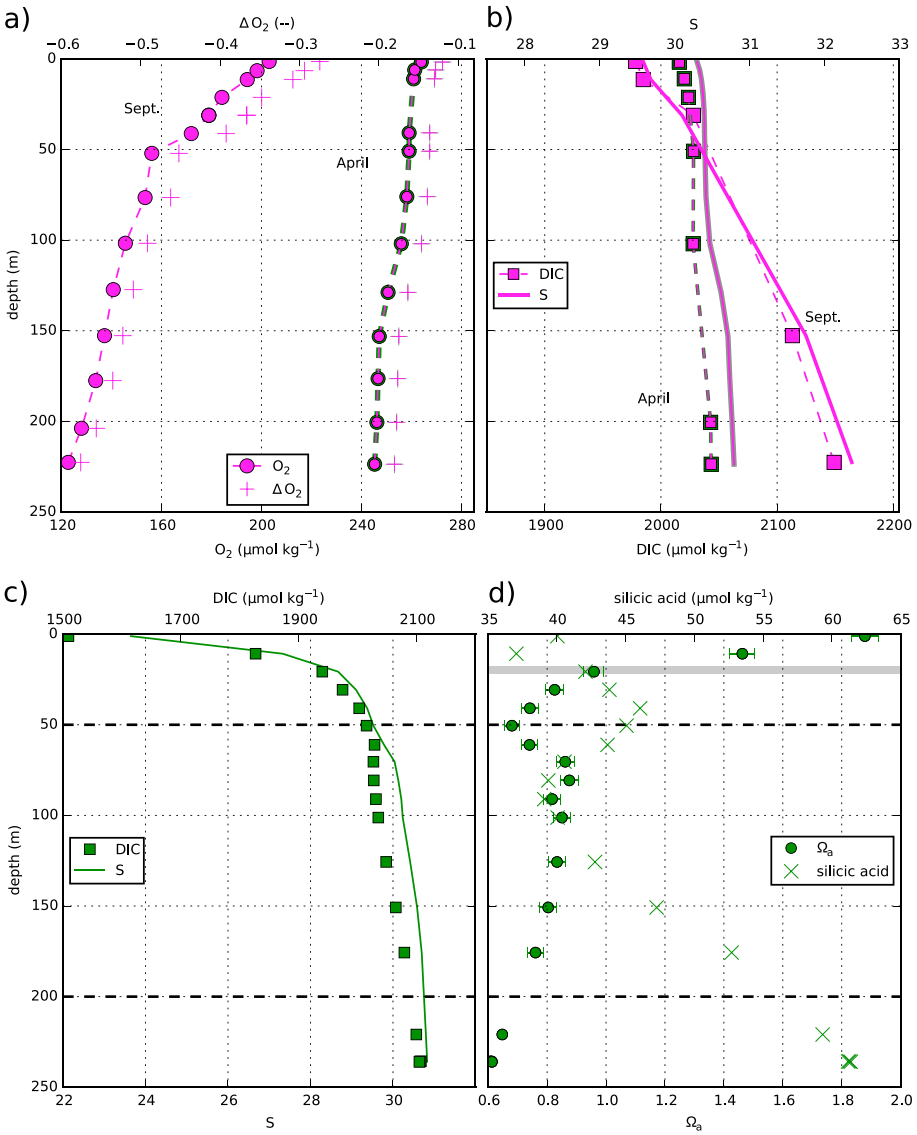

Figure 3. Vertical profiles of (a) O_2 (circle) and level of O_2 saturation, ΔO_2 (+). (b) DIC (square) and S (solid line) in Haro (48.63°N, 123.24°W, Figure 1) in spring (April 2012, darker purple) and late summer (September 2012, light purple). $\Delta O_2 = (O_2/O_{2eq} - 1)$, where *eq* indicates equilibrium (Text S3). Vertical profiles of (c) DIC (square) and S (solid line). (d) Ω_a (circle) and silicic acid (X) in S-SoG (49.15°N, 123.43°W) in July 2010 (weak FR year). The thick grey line marks the aragonite saturation horizon, and the SoG intermediate layer is between the dashed lines.

In contrast, the DIC inventory in Haro remains roughly constant (6.1×10^{11} mol) throughout the year (Table S4) and is primarily controlled by S (Figure 3b). This constancy is due in part to slow CO_2 gas exchange. Estimated CO_2 gas flux to the atmosphere in Haro is usually approximately an order of magnitude less than O_2 gas flux (into the ocean) throughout the year, even though surface CO_2 is almost always significantly farther from equilibrium with the atmosphere (8–90%) than O_2 (Table S4). In these data Haro surface O_2 undersaturation ranges from only 10 to 27%. Mixing is so vigorous that surface O_2 is always undersaturated (and CO_2 supersaturated) [*Murray et al.*, 2015], even when productivity is high in the SoG.

This intense mixing in Haro brings previously ventilated surface waters to depth [*Johannessen et al.*, 2014] and also allows significant absorption of O_2. We estimate that 1–6% of the O_2 deficit throughout the >200 m water column is erased (Table S4). This estimate does not include deep bubble injection near tidal fronts (up to 160 m in Haro). Local downwelling speeds ensure significant bubble dissolution, which will further enhance O_2 absorption and actually inject some CO_2 [*Baschek et al.*, 2006]. While total DIC inventories are an order of magnitude larger than O_2 inventories, the disequilibrium inventories (DIC surplus, O_2 deficit; Text S3)

are similar for each ($\sim 3 \times 10^{10}$ mol, Table S4). Therefore, gas exchange is not able to reduce the DIC surplus in Haro.

If subsurface oceanic O_2 decreases in the coming decades, then O_2 absorption in Haro may increase at times, as long as warming does not offset the increase in surface disequilibrium. On the other hand, atmospheric CO_2 is increasing rapidly, leading oceanic response, so the Haro DIC surplus (relative to the atmosphere) will decrease in the coming decades resulting in reduced CO_2 outgassing. In short, while the SoG is protected from hypoxia by gas exchange in Haro, it is not similarly protected from OA.

3.3. SoG Intermediate Water Renewal

Dynamic circulation in the SoG makes for complex vertical structure (Figures 3c and 3d). During summer and freshet, the FR-plume is characterized by high $Si(OH)_4$ and low S. In this brackish layer, changes in DIC are dominated by dilution/mixing. Just below, but still within the euphotic zone, S increases and $Si(OH)_4$ decreases (due in part to biological uptake). Below the euphotic zone, in the rest of the upper layer (top 50 m), nutrients and DIC increase and O_2 decreases with depth. The deep layer (below 200 m) is rich in $Si(OH)_4$ and DIC and has the lowest O_2 and pH in the water column.

Continual estuarine return flow from Haro occurs in the intermediate layer around 100 m [M06] but varies in depth depending on density (81 m, Figures 3c and 3d). This renewal causes local increases in S, decreases in DIC (grey line, Figure 2a), and significant decreases in $Si(OH)_4$. The estimation of Ω_a is sensitive to the DIC decrease, making the impact of this renewal on Ω_a striking; Ω_a increases by ~0.2 (Figure 3d) relative to the bottom of the upper layer (50 m). Similarly, pH increases by ~0.1 (not shown).

The properties of this incoming water are primarily controlled by those of the *d*JdF and the FR-plume [M06]. During summer, it is possible that each of these water masses serves to reduce DIC (raising pH) in the S-SoG intermediate layer, given the lower DIC content in the JdF (Figure 2a) and high productivity in the FR-plume. In winter, the contribution from the FR-plume is not likely to increase the intermediate layer pH (3.4.1).

3.3.1. Summer DIC End-Member Analysis

We investigated the potential of all four summer water masses to decrease DIC in this zone and gain insight into the overall DIC surplus in the SoG by considering their positions in DIC-S space (2.3). While the *d*JdF end-member contributes the most salt (by volume) to any mix of the four water masses, it is DIC poor. The deep SoG end-members sit ≥20 μmol kg^{-1} above the FR-plume:*d*JdF mixing line (Figure 2e and Table S5).

The FR-plume end-member is challenging to estimate. To ensure that biological drawdown was captured, we averaged S and DIC in the upper 15 m (following M06) in each summer and freshet profile (Text S4). Results highlight FR-plume variability (Table S6 and Figure 2e). Despite high FR-plume productivity, extrapolation of all potential FR-plume:*d*JdF mixing lines to S = 0 leads to positive DIC (210–670 μmol kg^{-1}). Thus, it appears that even though the subsurface North Pacific is enriched in carbon, the upwelled "acidified" outer shelf water [*Feely et al.*, 2008] plays the key role in raising local pH and saturation state when it enters the SoG at ~100 m.

The FR-plume end-member contains the most carbon during high freshet years (raised mixing lines, Table S6). The FR carries significant DIC (~900 μmol kg^{-1}) [*Moore-Maley*, 2014] and organic carbon [*Johannessen et al.*, 2003, 2015], part of which will remineralize to DIC somewhere in the system. The relative roles of FR carbon input, natural and anthropogenic, and high local organic matter production coupled with long retention times in the SoG require further investigation. The data indicate high DIC (and relatively low pH) throughout the SoG, not just in the deep water but also in the surface.

3.4. Surface pH and Aragonite Saturation Horizons

3.4.1. SoG

Surface conditions are variable and of immediate concern to aquaculture [*Haigh et al.*, 2015]. Surface pH in the SoG follows an intuitive seasonal cycle, highest in summer, when phytoplankton take up carbon, and lowest in winter when waters are well mixed and light limits production (Figure 4a). However, pH is most often lower than the global surface average, 8.1 [*The Royal Society*, 2005], despite strong blooms (one N-SoG datum, pH > 8.6).

During winter, surface pH throughout the SoG is ~7.8, similar to values reported in Puget Sound [*Feely et al.*, 2010], and the full water column is undersaturated with respect to aragonite (Figure 4), conditions that are deleterious to some larval and adult marine molluscs [*Waldbusser et al.*, 2015; *Bednarsek et al.*, 2014]. Surface undersaturation only ends with the advent of the spring bloom, when pH and Ω_a increase rapidly reaching 8.2 and 1.5, respectively, in the S-SoG [*Moore-Maley et al.*, 2016]. At this time, aragonite saturation horizons reach

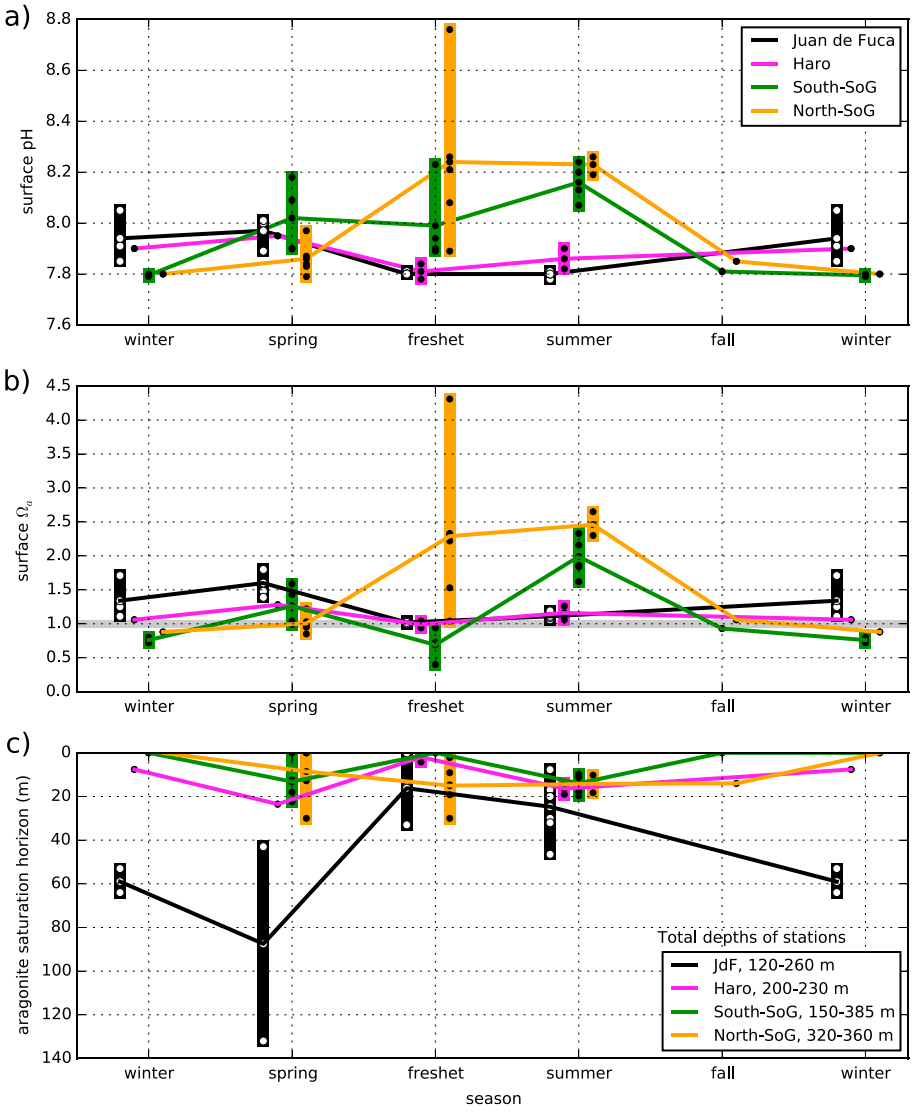

Figure 4. Seasonal surface (a) pH, (b) Ω_a (grey line indicates Ω_a = 1.0), and (c) aragonite saturation horizon for each region. Individual data (dots) are shown in an envelope colored by region. Lines connect seasonal means. Surface data are from the profile's top bottle; most (~70%) above 2 m; four data from 4–6 m, none of which are responsible for extremes in the ranges above.

their deepest level; only ~20 m in the S-SoG and slightly deeper in the N-SoG, ~30 m (Figure 4c), likely because there is less vertical estuarine entrainment and turbidity there, outside of the FR-plume. Many molluscs spend significant time at or below these depths (e.g., Geoduck clams, scallops, and pteropods) [*Haigh et al.*, 2015].

In Puget Sound summer aragonite saturation horizons appear to be deeper (30 to >100 m) [*Feely et al.*, 2010] than those in the SoG. On the outer BC shelf this horizon rarely (<1% of the time) gets as shallow as 20 m and the full water column is often *supersaturated* with respect to aragonite [*Lara-Espinosa*, 2013]. In contrast, at most 10–20% of the ~150–400 m water column is supersaturated in the SoG (Figure 4c).

During freshet conditions (surface S<20) pH drops to 7.9–8.0 and more dramatically, surface waters become undersaturated with respect to aragonite, producing low surface Ω_a (<0.5) in the S-SoG (Figure 4). This undersaturation results from dilution of calcium and carbonate ions and a decrease in primary productivity [*Moore-Maley et al.*, 2016].

3.4.2. Haro and JdF

The seasonal cycle in JdF and Haro is not intuitive; surface pH and Ω_a are higher in winter than in summer. This cycle is controlled by tidal mixing and outer coast circulation. Tidal mixing is so active that light is always

limiting to phytoplankton growth [*Mackas and Harrison*, 1997]. Therefore, the summer upwelling signature (high DIC) [*Ianson et al.*, 2003] is not erased by biology when it gets mixed into the surface in JdF and Haro. In contrast, winter downwelling brings offshore surface water, low in DIC (high pH) into JdF.

Surface properties are more consistent in these tidally mixed regions due to limited productivity. The highest surface pH (winter and spring) is ~7.9 in Haro, similar to values measured elsewhere in that region [*Murray et al.*, 2015] and ~8.0 in JdF (Figure 4a). Although these pH levels are not high, the surface is almost always saturated with respect to aragonite (Figure 4b). Meanwhile, the aragonite saturation horizon in JdF is variable (Figure 4c). Horizontal gradients are strong so this horizon becomes deeper in the seaward direction when multiple JdF sites are sampled. Also, vertical gradients are weak and the full water column is relatively close to saturation, so the "horizon" becomes blurred, similar to the tidally mixed zone at the entrance to Puget Sound [*Reum et al.*, 2014]. Finally, interannual variability is expected [e.g., *Masson and Cummins*, 2007].

4. Conclusions

Inorganic carbon is enriched throughout SoG waters relative to the JdF and Haro regions. As a result pH and Ω_a are generally low in the SoG, especially during winter when the full water column is undersaturated with respect to aragonite. Even in summer when productivity is high and surface pH is at its maximum (8.0–8.2), the saturation horizon is extremely shallow (~20 m), a shoaling that is almost never seen on the outer BC coast. During strong freshets the FR-plume causes surface undersaturation with respect to aragonite in the S-SoG by dilution and reduced productivity.

The regions connecting the SoG to the outer shelf (Haro and JdF) follow the opposite seasonal cycle with the highest pH, even at the surface, and deepest saturation horizons in winter and spring. This cycle is tied directly to the large-scale upwelling/downwelling circulation on the outer coast. Overall, these regions have higher Ω_a than the SoG, despite strong tidal mixing and light-limited productivity that result in relatively low (but less variable) surface pH (7.8–8.0) throughout the year.

Carbon levels are lower outside of the SoG, so estuarine return flow raises pH within the SoG. Most striking is the increase in pH and Ω_a around 100 m in the southern SoG where this return flow occurs. Of all water masses contributing to this return flow in summer, the "acidified" upwelled water from the outer coast is likely to increase pH most. While productive FR-plume water makes up about half of the return flow by volume, the biological DIC drawdown before mixing in Haro does not appear to be enough to reduce high FR-plume DIC, especially during strong freshets.

The O_2 content of upwelled waters entering the JdF is lower than anywhere in the SoG, even at depths greater than 300 m. Intense mixing in Haro protects the SoG from hypoxia by mixing down well-ventilated surface waters and allowing a significant uptake of O_2 via air-sea gas exchange. In contrast, CO_2 gas exchange is slow, and the outgassing of carbon in Haro is insignificant. In the coming decades, as atmospheric CO_2 increases rapidly, this flux will only decrease and perhaps even change direction. Meanwhile, O_2 uptake in Haro may increase, as long as T does not increase too rapidly. Thus, the SoG is protected from hypoxia but is particularly vulnerable to OA. We suggest that these results may apply broadly to estuarine regions with restricted exchange where tidal mixing is intense.

Acknowledgments
We thank Diane Masson and Peter Chandler for accommodating our work on their cruises, Marty Davelaar for sample analysis, and Andrew Dickson, Simone Alin, Richard Feely, and Paul Covert for helpful conversations concerning the challenges of collecting data in estuarine environments. We are grateful for the helpful comments of Wei-Jun Cai and an anonymous reviewer. This work was funded by Fisheries and Oceans Canada's International Governance Strategy. All data appear in figures, and all calculations are explicitly described; the raw data may be obtained from D.I. (debby.ianson@dfo-mpo.gc.ca).

References

Azetsu-Scott, K., M. Starr, Z.-P. Mei, and M. Granskog (2014), Low calcium carbonate saturation state in an Arctic inland sea having large and varying fluvial inputs: The Hudson Bay system, *J. Geophys. Res. Oceans*, *119*, 6210–6220, doi:10.1002/2014JC009948.

Baschek, B., D. M. Farmer, and C. Garrett (2006), Tidal fronts and their role in air-sea gas exchange, *J. Mar. Res.*, *64*, 483–515, doi:10.1357/002224006778715766.

Bednarsek, N., R. A. Feely, J. C. P. Reum, B. Peterson, J. Menkel, S. R. Alin, and B. Hales (2014), Limacina helicina shell dissolution as an indicator of declining habitat suitability owing to ocean acidification in the California Current ecosystem, *Proc. R. Soc. B*, *281*(1785), 20140123, doi:10.1098/rspb.2014.0123.

Bylhouwer, B., D. Ianson, and K. Kohfeld (2013), Changes in the onset and intensity of wind-driven coastal upwelling and downwelling along the North American Pacific coast, *J. Geophys. Res. Oceans*, *118*, 2565–2580, doi:10.1002/jgrc.20194.

Cai, W.-J., et al. (2011), Acidification of subsurface coastal waters enhanced by eutrophication, *Nat. Geosci.*, *4*(11), 766–770, doi:10.1038/ngeo1297.

Davis, K. A., N. S. Banas, S. N. Giddings, S. A. Siedlecki, P. MacCready, E. J. Lessard, R. M. Kudela, and B. M. Hickey (2014), Estuary-enhanced upwelling of marine nutrients fuels coastal productivity in the U.S. Pacific Northwest, *J. Geophys. Res. Oceans*, *119*, 8778–8799, doi:10.1002/2014JC010248.

Ekstrom, J. A., et al. (2015), Vulnerability and adaptation of us shellfisheries to ocean acidification, *Nat. Clim. Change*, *5*(3), 207–214, doi:10.1038/nclimate2508.

Emerson, S., and J. Hedges (2008), *Chemical Oceanography and the Marine Carbon Cycle*, p. 453, Cambridge Univ. Press, Cambridge, U. K.
Farmer, D., R. Pawlowicz, and R. Jiang (2002), Tilting separation flows: A mechanism for intense vertical mixing in the coastal ocean, *Dyn. Atmos. Oceans*, *36*, 43–58, doi:10.1016/S0377-0265(02)00024-6.
Feely, R. A., C. L. Sabine, J. M. Hernandez-Ayon, D. Ianson, and B. Hales (2008), Evidence for upwelling of corrosive 'acidified' water onto the continental shelf, *Science*, *320*, 1490–1492, doi:10.1126/science.155676.
Feely, R. A., S. R. Alin, C. L. Sabine, M. Warner, A. Devol, C. Krembs, and C. Maloy (2010), The combined effects of ocean acidification, mixing and respiration on pH and carbonate saturation in an urbanized estuary, *Estuarine Coastal Shelf Sci.*, *88*, 442–449.
Gruber, N. (2011), Warming up, turning sour, losing breath: Ocean biogeochemistry under global change, *Philos. Trans. R. Soc. A*, *369*(1943), 1980–1996, doi:10.1098/rsta.2011.0003.
Haigh, R., D. Ianson, C. A. Holt, H. E. Neate, and A. M. Edwards (2015), Effects of ocean acidification on temperate coastal marine ecosystems and fisheries in the northeast Pacific, *PLoS One*, *10*(2), e0117533, doi:10.1371/journal.pone.0117533.
Harrison, P. J., J. D. Fulton, F. J. R. Taylor, and T. R. Parsons (1983), Review of the biological oceanography of the Strait of Georgia: Pelagic environment, *Can. J. Fish. Aquat. Sci.*, *40*(7), 1064–1094, doi:10.1139/f83-129.
Hu, X., and W.-J. Cai (2013), Estuarine acidification and minimum buffer zone—A conceptual study, *Geophys. Res. Lett.*, *40*, 5176–5181, doi:10.1002/grl.51000.
Ianson, D., S. Harris, S. E. Allen, K. Orians, D. Varela, and C. S. Wong (2003), The inorganic carbon system in the coastal upwelling region west of Vancouver Island, Canada, *Deep Sea Res., Part I*, *50*, 1023–1042.
Intergovernmental Panel on Climate Change (2011), *Workshop Report of the Intergovernmental Panel on Climate Change Workshop on Impacts of Ocean Acidification on Marine Biology and Ecosystems*, p. 164, Working Group II Tech. Support Unit, Carnegie Inst., Stanford, USA.
Johannessen, S. C., R. W. Macdonald, and D. W. Paton (2003), A sediment and organic carbon budget for the greater Strait of Georgia, *Estuarine Coastal Shelf Sci.*, *56*, 845–860, doi:10.1016/S0272-7714(02)00303-7.
Johannessen, S. C., D. Masson, and R. W. Macdonald (2014), Oxygen in the deep strait of Georgia, 1951–2009: The roles of mixing, deep-water renewal, and remineralization of organic carbon, *Limnol. Oceanogr.*, *59*(1), 211–222, doi:10.4319/lo.2014.59.1.0211.
Johannessen, S. C., R. W. Macdonald, B. Burd, A. van Roodselaar, and S. Bertold (2015), Local environmental conditions determine the footprint of municipal effluent in coastal waters: A case study in the Strait of Georgia, British Columbia, *Sci. Total Environ.*, *508*, 228–239, doi:10.1016/j.scitotenv.2014.11.096.
Lara-Espinosa, A. (2013), Determination of the acidification state of Canadian Pacific coastal waters using empirical relationships with hydrographic data, Master's thesis, Univ. of Victoria, Victoria, Canada.
LeBlond, P. H. (1983), The Strait of Georgia: Functional anatomy of a coastal sea, *Can. J. Fish. Aquat. Sci.*, *40*, 1033–1063.
Mackas, D. L., and P. J. Harrison (1997), Nitrogenous nutrient sources and sinks in the Juan de Fuca Strait/Strait of Georgia/Puget Sound estuarine system: Assessing the potential for eutrophication, *Estuarine Coastal Shelf Sci.*, *44*(1), 1–21, doi:10.1006/ecss.1996.0110.
Masson, D. (2002), Deep water renewal in the Strait of Georgia, *Estuarine Coastal Shelf Sci.*, *54*(1), 115–126, doi:10.1006/ecss.2001.0833.
Masson, D. (2006), Seasonal water mass analysis for the Straits of Juan de Fuca and Georgia, *Atmos. Ocean*, *44*, 1–15.
Masson, D., and P. F. Cummins (2007), Temperature trends and interannual variability in the Strait of Georgia, British Columbia, *Cont. Shelf Res.*, *27*(5), 634–649, doi:10.1016/j.csr.2006.10.009.
Moore-Maley, B. (2014), The inorganic carbonate chemistry of the southern Strait of Georgia, Master's thesis, Univ. of British Columbia, British Columbia, Canada.
Moore-Maley, B. L., S. E. Allen, and D. Ianson (2016), Locally driven interannual variability of near-surface pH and Ω_A in the Strait of Georgia, *J. Geophys. Res. Oceans*, *121*, 1600–1625, doi:10.1002/2015JC011118.
Murray, J. W., E. Roberts, E. Howard, M. O'Donnell, C. Bantam, E. Carrington, M. Foy, B. Paul, and A. Fay (2015), An inland sea high nitrate-low chlorophyll (HNLC) region with naturally high pCO_2, *Limnol. Oceanogr.*, *60*(3), 957–966, doi:10.1002/lno.10062.
Pawlowicz, R., O. Riche, and M. Halverson (2007), The circulation and residence time of the Strait of Georgia using a simple mixing-box approach, *Atmos. Ocean*, *45*(4), 173–193, doi:10.3137/ao.450401.
Reum, J. C. P., S. R. Alin, R. A. Feely, J. Newton, M. Warner, and P. McElhany (2014), Seasonal carbonate chemistry covariation with temperature, oxygen, and salinity in a fjord estuary: Implications for the design of ocean acidification experiments, *PLoS ONE*, *9*(2), e89619, doi:10.1371/journal.pone.0089619.
Seibel, B. A. (2011), Critical oxygen levels and metabolic suppression in oceanic oxygen minimum zones, *J. Exp. Biol.*, *214*, 326–336, doi:10.1242/jeb.049171.
The Royal Society (2005), *Ocean Acidification Due To Increasing Atmospheric Carbon Dioxide*, p. 68, Clyvedon Press, Cardiff, U. K.
Voss, B. M., et al. (2014), Tracing river chemistry in space and time: Dissolved inorganic constituents of the Fraser River, Canada, *Geochim. Cosmochim. Acta*, *124*, 283–308, doi:10.1016/j.gca.2013.09.006.
Waldbusser, G. G., and J. E. Salisbury (2014), Ocean acidification in the coastal zone from an organism's perspective: Multiple system parameters, frequency domains, and habitats, *Annu. Rev. Mar. Sci.*, *6*(1), 221–247, doi:10.1146/annurev-marine-121211-172238.
Waldbusser, G. G., B. Hales, C. J. Langdon, B. A. Haley, P. Schrader, E. L. Brunner, M. W. Gray, C. A. Miller, and I. Gimenez (2015), Saturation-state sensitivity of marine bivalve larvae to ocean acidification, *Nat. Clim. Change*, *5*, 273–280, doi:10.1038/nclimate2479.
Zhai, W. D., M. Dai, and W.-J. Cai (2009), Coupling of surface pCO_2 and dissolved oxygen in the northern South China Sea: Impacts of contrasting coastal processes, *Biogeosciences*, *6*(11), 2589–2598, doi:10.5194/bg-6-2589-2009.